fluids

MDPI

Article

Extraction of Tangential Momentum and Normal Energy Accommodation Coefficients by Comparing Variational Solutions of the Boltzmann Equation with Experiments on Thermal Creep Gas Flow in Microchannels

Tommaso Missoni [1], Hiroki Yamaguchi [2], Irina Graur [3,*] and Silvia Lorenzani [1]

[1] Dipartimento di Matematica, Politecnico di Milano, Piazza Leonardo da Vinci 32, 20133 Milano, Italy; tommaso.missoni@mail.polimi.it (T.M.); silvia.lorenzani@polimi.it (S.L.)
[2] Department of Micro-Nano Mechanical Science and Engineering, Nagoya University, Furo-cho, Chikusa, Nagoya 464-8603, Aichi, Japan; hiroki@nagoya-u.jp
[3] Aix-Marseille Université, CNRS IUSTI UMR 7343, 5 Rue Enrico Fermi, 13453 Marseille, France
* Correspondence: irina.martin@univ-amu.fr

Abstract: In the present paper, we provide an analytical expression for the first- and second-order thermal slip coefficients, $\sigma_{1,T}$ and $\sigma_{2,T}$, by means of a variational technique that applies to the integrodifferential form of the Boltzmann equation based on the true linearized collision operator for hard-sphere molecules. The Cercignani-Lampis scattering kernel of the gas-surface interaction has been considered in order to take into account the influence of the accommodation coefficients (α_t, α_n) on the slip parameters. Comparing our theoretical results with recent experimental data on the mass flow rate and the slip coefficient for five noble gases (helium, neon, argon, krypton, and xenon), we found out that there is a continuous set of values for the pair (α_t, α_n) which leads to the same thermal slip parameters. To uniquely determine the accommodation coefficients, we took into account a further series of measurements carried out with the same experimental apparatus, where the thermal molecular pressure exponent γ has been also evaluated. Therefore, the new method proposed in the present work for extracting the accommodation coefficients relies on two steps. First of all, since γ mainly depends on α_t, we fix the tangential momentum accommodation coefficient in such a way as to obtain a fair agreement between theoretical and experimental results. Then, among the multiple pairs of variational solutions for (α_t, α_n), giving the same thermal slip coefficients (chosen to closely approximate the measurements), we select the unique pair with the previously determined value of α_t. The analysis carried out in the present work confirms that both accommodation coefficients increase by increasing the molecular weight of the considered gases, as already highlighted in the literature.

Keywords: Boltzmann equation; hard-sphere molecules; Cercignani-Lampis scattering kernel; thermal slip coefficients; thermal molecular pressure exponent

Citation: Missoni, T.; Yamaguchi, H.; Graur, I.; Lorenzani, S. Extraction of Tangential Momentum and Normal Energy Accommodation Coefficients by Comparing Variational Solutions of the Boltzmann Equation with Experiments on Thermal Creep Gas Flow in Microchannels. *Fluids* **2021**, *6*, 445. https://doi.org/10.3390/fluids6120445

Academic Editor: Mehrdad Massoudi

Received: 1 November 2021
Accepted: 2 December 2021
Published: 9 December 2021

1. Introduction

From the pioneering works of Reynolds [1], Maxwell [2] and Knudsen [3,4] it is known that a gas flow is generated through a capillary if the temperature is different at its ends, and this flow is directed toward the hot extremity of the capillary. This phenomenon is called the thermal transpiration or thermal creep and the mass flow rate generated by applying a temperature gradient along the capillary walls is called the temperature driven mass flow rate, denoted in the following by M_{T}. If the capillary is settled between two reservoirs of finite volumes maintained at different temperatures and initially at the same pressure, first a temperature driven flow is generated from the cold to the hot side, then it is counterbalanced by the Poiseuille flow, denoted in the following by M_{P}, since the pressure in the hot reservoir becomes higher than in the cold one. The system comes to an

equilibrium when the Poiseuille mass flow rate matches the temperature driven mass flow rate, $M_P = M_T$, making the total mass flow rate between the reservoirs equal to zero. The pressure difference between the reservoirs, which corresponds to this final stage, is called the *Thermal molecular Pressure Difference (TPD).* These phenomena become important when a gas flowing through a capillary is rarefied, i.e., the ratio between the molecular mean free path, λ, and a characteristic flow dimension, a, (in this case the capillary radius) called the Knudsen number, $Kn = \lambda/a$, is larger than 0.01. Since the Knudsen number is defined as the ratio between two quantities, λ and a, it could be relatively large either when the molecular mean free path is large (low pressure) or when the characteristic flow dimension is small (gas flows in the microsystems). Therefore, the thermal creep phenomenon is important either at low pressure or for the gas flows at small scales.

In the last decades, the property of the TPD generation, due to a temperature gradient applied to a surface, started to be used for the development of microdevices like micro gas sensors [5,6], micropumps without moving parts and lubricant fluids [7–10] and micro gas chromatography columns [11–13]. The information about the TPD can also be used to calculate several physical quantities as the Eucken factor, the rotational collision number [14] and the heat conductivities of polar and non-polar polyatomic gases [15].

However, the thermal molecular pressure difference has also a negative effect in the accuracy of the pressure measurements. For example, in order to minimize the zero drift, some of Capacitance Diaphragm Gauges (CDG) are operated keeping the sensor at a higher temperature [16]. This difference in the temperature between the sensor and the vacuum chamber makes the behavior of the gauge non-linear due to thermal transpiration effects and the pressure readings have to be corrected. The same effect needs to be taken into account when the vapor-pressure thermometry or gas thermometry techniques are used to measure the temperature below 0 °C [17], due to a large difference in temperature between the vessels where the pressure is measured.

The thermal molecular pressure difference effect depends on several factors [17]: the nature of the gas and in particular its thermal conductivity; the absolute pressure value; the flow regime (hydrodynamic, transitional or free molecular); the temperature values or the mean temperature and the temperature gradient between the cold and the hot measurement points; the material and the state of the internal surface of the connecting tube.

If one considers all the applications described above, it is clear that an accurate prediction of the TPD is very important in practice. Relying on the results of the kinetic theory, Reynolds pointed out [1] that in the free molecular flow regime the pressure ratio between the cold and the hot reservoirs is proportional to the square root of the respective reservoir temperatures:

$$\frac{p_c}{p_h} = \left(\frac{T_c}{T_h}\right)^{1/2}, \tag{1}$$

where p_c and p_h are the pressures in the cold and the hot reservoirs, respectively; T_c and T_h are the corresponding temperatures. Equation (1) has been derived for two reservoirs connected by an orifice and the probabilities for the molecules to traverse the orifice are equal on its both sides. However, more often, a capillary connects two reservoirs. In this case, the mentioned probability, to a great extent, depends on the surface properties of the tube where the gas molecules collide and on the degree of energy exchange. Under these conditions, the pressure ratio p_c/p_h will be smaller than the ratio predicted by Equation (1) [18]

$$\frac{p_c}{p_h} = \left(\frac{T_c}{T_h}\right)^{\gamma}. \tag{2}$$

In the above formula, the ratio p_c/p_h is usually called the Thermal molecular Pressure Ratio (TPR) and the factor γ is called the Thermal molecular Pressure Exponent (TPE).

It is difficult to derive a reliable and universal expression based on a well-established theory of the thermal molecular pressure difference effect, in particular in the transitional region, which represents an intermediate regime between the low pressure free molecular

flow limit (where Equation (2) can be used) and the high pressure hydrodynamic flow regime (where Equation (2) reduces to $p_c = p_h$).

Maxwell was the first to propose an analytical expression [2] for the mass flow through a capillary driven by the pressure and temperature gradients. He introduced the concepts of the slip velocity and of the accommodation coefficient, the latter to describe the processes involved in the gas-surface interaction. The formula derived by Maxwell allows one to calculate the TPD assuming the zero final mass flow rate, but it is valid only in the hydrodynamic and slip flow regimes. Later, Knudsen measured the thermal molecular pressure difference of hydrogen at different gas rarefaction conditions and proposed the improved semi-empirical expression for the TPD [3,19], satisfying the two limits: Equation (1) in the free molecular flow regime and the zero TPD in the hydrodynamic region. Several researchers followed the ideas of Knudsen and proposed various semi-empirical formulas to calculate the TPD [20–24].

From the experimental results on the thermal molecular pressure difference reported in [25], it became clear that the Maxwell model for the complete diffuse reflection of the gas molecules from a surface was inappropriate to predict the thermal transpiration phenomenon at arbitrary Knudsen numbers. The author of Ref. [25] extracted the accommodation coefficient from the experimental data by fitting the expressions for the pressure and temperature driven mass flow rates proposed by Maxwell with a least square method and found that this value is different from 1. However, these results have shown that the thermal molecular pressure difference has little or no dependence on the gas-surface interaction: all the tested gases converged towards the same value. These findings were in good agreement with those reported in Ref. [26], where the thermal transpiration problem was analyzed numerically with arbitrary accommodation at the surface, always in the frame of the Maxwell diffuse-specular kernel.

Applying the Maxwell scattering kernel to calculate the TPD in the free-molecular regime, one obtains that the exponent γ is equal to 0.5 for any value of the accommodation coefficient. However, the authors of Ref. [27], by studying experimentally the thermal transpiration flow with ultrahigh vacuum techniques, concluded that the theoretical value of $\gamma = 0.5$, predicted by Reynolds (Equation (1)) is effectively never reached and that lower values of γ, between 0.4 and 0.5, are possible.

The application of a more realistic scattering kernel, compared to the Maxwell one, as the Cercignani-Lampis (CL) model, allows one to improve the understanding of the gas-wall interaction properties for thermal creep flows. The author of Ref. [28] applied the Cercignani-Lampis boundary conditions to the linearized Shakhov kinetic model to simulate a flow through a long tube of circular cross section. It has been found that the values of γ are less sensitive to the variation of α_n than of α_t. Thus, the tangential momentum accommodation coefficient α_t has been extracted from the measurements of γ, given in [29] for various gases in a glass capillary, assuming that the normal energy accommodation coefficient, α_n, is equal to 1. In this way, a good agreement has been obtained between the measured and simulated values of γ for helium, neon, argon and xenon. However, in the framework of the Cercignani-Lampis model of boundary conditions, reliable values of the normal energy accommodation coefficient α_n are rare. A standard procedure used up to now consists of fixing the value of α_n and then in fitting the experimental data to obtain the value of α_t, as done in Ref. [28]. In a recent paper [30], the values of α_n, extracted from the literature of measurements of the acoustic resonance frequencies of helium-filled and argon-filled spherical metal cavities, have been reported. The Shakhov kinetic model with the Cercignani-Lampis boundary conditions has been solved in order to reproduce the temperature jump coefficient determined in these experiments. The numerical results have revealed that a continuous set of values of α_t and α_n can lead to the same jump coefficient. Therefore, to be able to uniquely estimate α_n, one should use additional information about α_t, exploiting other methods of measurement different from the acoustic resonance. As a consequence, the authors of [30] have reported the values of α_t and α_n for helium and argon determined in diverse experimental settings. In the above cited works, the correlation

between the measurements and the theoretical results has been analyzed in a narrow range of the rarefaction parameter (typically the near-continuum regime or the free-molecular flow limit where analytical formulas can be derived for the particular problem at hand).

Recently, in Ref. [31], the thermal-creep problem of a rarefied gas between two parallel plates has been investigated by using a variational approach that applies to the integrodifferential form of the linearized Boltzmann equation for hard-sphere molecules. In the frame of the Cercignani-Lampis boundary conditions, new analytical expressions for the first- and second-order thermal slip coefficients have been derived in terms of the tangential momentum α_t and the normal energy α_n accommodation coefficients. These theoretical results have been compared with the thermal slip parameters experimentally measured by the authors of Ref. [32]. For five noble gases, the values of α_t and α_n have been extracted and then used to evaluate the temperature-driven mass flow rates. A good agreement has been obtained between the variational outputs and the experimental data. However, as already underlined in [30], for some specific values of the thermal-slip coefficients, there can exist multiple solutions for the accommodation coefficients.

The main objective of this work is to extend the previous findings reported in [31] and to propose a methodology to uniquely determine α_t and α_n.

2. The Variational Approach to Plane Poiseuille and Thermal-Creep Problems

Let us consider two infinite parallel plates separated by a distance d and a gas flowing between them, in the z-direction, owing to longitudinal gradients of pressure and temperature defined as follows:

$$k = \frac{1}{p}\frac{\partial p}{\partial z}, \qquad \tau = \frac{1}{T}\frac{\partial T}{\partial z} \tag{3}$$

with p and T being the local gas pressure and temperature, respectively. Both walls are fixed at $x = \pm d/2$. If the pressure and temperature gradients are taken to be small, the Boltzmann equation can be linearized [31]:

$$c_x \frac{\partial h}{\partial x} + k c_z + \tau c_z \left(c^2 - \frac{5}{2} \right) = Lh, \tag{4}$$

where $h(x, \mathbf{c})$ is the small perturbation on the basic equilibrium state, $\mathbf{c}$ is the molecular velocity vector expressed in units of $(2RT)^{1/2}$ (with R being the specific gas constant) and Lh is the linearized collision operator. In the following, we study the Poiseuille and thermal-creep flows on the basis of the linearized Boltzmann equation for hard-sphere molecules. This approach provides a better approximation of real-gas behavior than commonly used kinetic models, as the Bhatnagar-Gross-Krook (BGK) or the Shakhov (S) models. The Boltzmann Equation (4) can be solved with appropriate boundary conditions imposed on the walls of the channel. Once the distribution function h is evaluated, the bulk velocity of the gas $v_z(x)$ and the heat flux $q_z(x)$ can be calculated as

$$v_z(x) = \pi^{-\frac{3}{2}} \int_{-\infty}^{+\infty} \int_{-\infty}^{+\infty} \int_{-\infty}^{+\infty} e^{-c^2} c_z h(x, \mathbf{c})\, d\mathbf{c}, \tag{5}$$

$$q_z(x) = \pi^{-\frac{3}{2}} \int_{-\infty}^{+\infty} \int_{-\infty}^{+\infty} \int_{-\infty}^{+\infty} e^{-c^2} c_z \left(c^2 - \frac{5}{2} \right) h(x, \mathbf{c})\, d\mathbf{c}. \tag{6}$$

Hence, the mass $\dot{M}$ and heat $\dot{Q}$ flow rates (per unit time through unit thickness) read

$$\dot{M} = \rho \int_{-d/2}^{d/2} v_z(x) dx, \tag{7}$$

$$\dot{Q} = \int_{-d/2}^{d/2} q_z(x) dx, \tag{8}$$

where ρ is the gas density. To apply the variational formulation, we shall rewrite Equation (4) in the following symbolic form:

$$(D - L)h = S, \tag{9}$$

where $Dh = c_x \frac{\partial h}{\partial x}$ and $S = -c_z k - c_z \left(c^2 - \frac{5}{2} \right) \tau$. The boundary conditions to be matched with Equation (9) have the general expression

$$h^+ = Kh^-, \tag{10}$$

where h^+ and h^- concern the reemitted and the impinging molecules on the boundaries, respectively, and the operator K depends on the scattering kernel used. In this work, we consider the Cercignani-Lampis (CL) boundary conditions [33] based on two different adjustable parameters: α_t, which is the accommodation coefficient of the tangential momentum ($\alpha_t \in [0, 2]$) and α_n, which is the accommodation of the kinetic energy owing to the velocity normal to the bounding walls ($\alpha_n \in [0, 1]$). This model provides a more realistic physical description of the gas-surface interaction, compared to the most popular Maxwell diffuse-specular scattering kernel with only one adjustable parameter. The CL boundary conditions take the form:

$$h^+(-(d/2)\mathrm{sgn}c_x, \mathbf{c}) = \int_{c'_x<0} R_{CL}(-\mathbf{c} \to -\mathbf{c}')\, h^-(-(d/2)\mathrm{sgn}c_x, \mathbf{c}')\, d\mathbf{c}', \tag{11}$$

where

$$R_{CL}(\mathbf{c}' \to \mathbf{c}) = \frac{2c_x}{\pi \alpha_t \alpha_n (2 - \alpha_t)} \exp\left\{ - \frac{[\mathbf{c}_t - (1 - \alpha_t)\mathbf{c}'_t]^2}{\alpha_t (2 - \alpha_t)} \right\} \times \exp\left\{ - \frac{[{c_x}^2 + (1 - \alpha_n){c'_x}^2]}{\alpha_n} \right\} I_o\left(\frac{2\sqrt{1 - \alpha_n}}{\alpha_n} c_x c'_x \right), \tag{12}$$

with $\mathbf{c}_t = (c_y, c_z)$ being the two-dimensional vector of the tangential molecular velocity and I_o being the modified Bessel function of first kind and zeroth order. Let us now introduce the following functional J of the test function $\tilde{h}$ [34,35]:

$$J(\tilde{h}) = ((\tilde{h}, P(D\tilde{h} - L\tilde{h}))) - 2((PS, \tilde{h})) + (\tilde{h}^+ - K\tilde{h}^-, P\tilde{h}^-)_B, \tag{13}$$

where P is the parity operator in velocity space, defined by $P[h(\mathbf{c})] = h(-\mathbf{c})$, while $((,))$, $(,)_B$ denote two scalar products:

$$((h, g)) = \pi^{-3/2} \int_{-d/2}^{+d/2} \int_{-\infty}^{+\infty} \exp(-c^2) h(x, \mathbf{c}) g(x, \mathbf{c})\, d\mathbf{c} dx \tag{14}$$

$$(h^\pm, g^\pm)_B = \pi^{-3/2} \int_{\partial\Omega} \int_{c_x>0} c_x \exp(-c^2) h^\pm(\mathbf{c}) g^\pm(\mathbf{c})\, d\mathbf{c} d\sigma\,. \tag{15}$$

In the one-dimensional case, the integration over the boundary $\partial\Omega$ reduces to the sum of the terms at $x = \pm d/2$.

Using the variational principle described in Refs. [34,35], one can prove that the functional $J(\tilde{h})$ attains its stationary (minimum) value when $\tilde{h} = h(x, \mathbf{c})$ solves Equation (9) with the boundary conditions (10). If we let $\tilde{h} = h$, Equation (13) reduces to:

$$J(h) = -((PS, h)) = -k \int_{-d/2}^{d/2} v_z(x) dx - \tau \int_{-d/2}^{d/2} q_z(x) dx = -k \frac{\dot{M}}{\rho} - \tau \dot{Q}. \tag{16}$$

Thus, the stationary value of J has a direct connection with the quantities of physical interest. For linearized problems, the mass and heat flow rates, per unit width, can be written as the sum of the Poiseuille and thermal-creep contributions:

$$\dot{M} = d^2\, p\, [-G_p\, k + G_T\, \tau], \tag{17}$$

$$\dot{Q} = \frac{d^2}{2}\, p\, [Q_p\, k - Q_T\, \tau], \tag{18}$$

where G_p, G_T, Q_p and Q_T are positive dimensionless coefficients that represent the Poiseuille coefficient, the thermal-creep coefficient, the mechanocaloric coefficient and the reduced heat flux, respectively. One can prove that the cross coefficients, G_T and Q_p, satisfy the Onsager relation [36–38]:

$$G_T = Q_p. \tag{19}$$

Following the general method presented in [39] we derived an accurate expression for the trial function $\tilde{h}(x, \mathbf{c})$ by considering the solution of the BGK-Boltzmann equation in integral form for the coupled Poiseuille and thermal-creep problems. In this formula, the bulk velocity profile has been approximated by

$$\tilde{v}_z(x) = Ax^2 + C \tag{20}$$

with the adjustable constants A and C being represented as:

$$A = A_p + A_T, \quad C = C_p + C_T \tag{21}$$

due to the linear superposition of the Poiseuille and thermal-creep effects. Since the solution of the BGK-Boltzmann equation, valid for all rarefaction regimes, contains exponential functions (describing the Knudsen layers) which cannot be easily manipulated in an analytical way within the framework of the true linearized collision operator, the following simplified test function has been used to evaluate Equation (13):

$$\tilde{h}(x, \mathbf{c}) = 2Ac_z(x^2 - 2xc_x\theta + 2{c_x}^2\theta^2) + 2c_z\left(C - \frac{k\theta}{2}\right) - B\tau\theta c_z\left(c^2 - \frac{5}{2}\right). \tag{22}$$

In Equation (22), A, B and C are adjustable constants to be varied in order to obtain the best value of $J(\tilde{h})$, and θ is a length parameter that will be specified in the following. Due to the simplifications carried out in deriving Equation (22), the range of validity of the variational results extends into the transitional and near-continuum flow regimes. The trial function (22) shows the same dependence on x and $\mathbf{c}$ as the asymptotic form of the test function derived in [36] via the use of the Chapman-Enskog procedure. Let us now rescale the constant A appearing in Equation (22) as follows: $A = \frac{A}{\theta^2}$, and define the rarefaction parameter (inverse Knudsen number):

$$\delta = \frac{d}{\theta}. \tag{23}$$

For molecules approximated by hard spheres of diameter σ, the length parameter θ is given by $\theta = \sqrt{2}/(\pi^{3/2}\sigma^2 n)$, where n is the gas number density. Substituting $\tilde{h}$, given by Equation (22), in Equation (13) and splitting the constants as in Equation (21), with the normalization

$$\hat{A}_p = \frac{A_p}{(k\theta)}, \quad \hat{C}_p = \frac{C_p}{(k\theta)}, \quad \hat{A}_T = \frac{A_T}{(\tau\theta)}, \quad \hat{C}_T = \frac{C_T}{(\tau\theta)} \tag{24}$$

the functional $J(\tilde{h})$ reduces to the sum of three functionals: $J^{(1)}(\tilde{h})$, $J^{(2)}(\tilde{h})$, $J^{(3)}(\tilde{h})$, simply grouping together the terms proportional to $(k\theta)^2$, $(\tau\theta)^2$ and $(k\theta)(\tau\theta)$, respectively. Each

functional is a polynomial of the second order with respect to the constants A_p, A_T, B, C_p and C_T, that are to be determined:

$$J^{(1)}(\tilde{h})/(k\theta)^2 = (\sqrt{\pi})^{-1} \times \left\{ \frac{c_{11}}{2} A_p^2 + \frac{c_{22}}{2} C_p^2 + c_{12} A_p C_p - c_1 A_p - c_2 C_p + \frac{1}{2}(c_2 - c_{22}/4) \right\}, \quad (25)$$

$$J^{(2)}(\tilde{h})/(\tau\theta)^2 = (\sqrt{\pi})^{-1} \times \left\{ \frac{c_{11}}{2} A_T^2 + \frac{d_{22}}{2} B^2 + \frac{c_{22}}{2} C_T^2 + d_{12} A_T B + c_{12} A_T C_T - d_1 A_T - d_2 B + d_{23} B C_T \right\}, \quad (26)$$

$$J^{(3)}(\tilde{h})/[(k\theta)(\tau\theta)] = (\sqrt{\pi})^{-1} \times \left\{ c_{11} A_p A_T + c_{22} C_p C_T + c_{12}(A_p C_T + A_T C_p) - d_1 A_p - c_1 A_T - c_2 C_T + d_{12} A_p B + d_{23} B C_p - \frac{d_{23}}{2} B \right\}. \quad (27)$$

The nondimensional coefficients appearing in Equations (25)–(27) have been explicitly reported in [31]. The derivatives of $J^{(1)}(\tilde{h})/(k\theta)^2$, $J^{(2)}(\tilde{h})/(\tau\theta)^2$, and $J^{(3)}(\tilde{h})/[(k\theta)(\tau\theta)]$, with respect to A_p, A_T, B, C_p and C_T vanish in correspondence of the optimal values of these constants [31].

Since the functional J can be split into three parts and the relations (16)–(18) hold, it is easy to see that the computation of the minimum of $J^{(1)}(\tilde{h})/(k\theta)^2$, $J^{(2)}(\tilde{h})/(\tau\theta)^2$ and $J^{(3)}(\tilde{h})/[(k\theta)(\tau\theta)]$ will lead to an accurate estimate of the Poiseuille coefficient G_p, the thermal-creep coefficient G_T, and the reduced heat flux Q_T:

$$G_p = \frac{2}{\delta^2} \min \frac{J^{(1)}(\tilde{h})}{(k\theta)^2}, \quad (28)$$

$$G_T = -\frac{1}{\delta^2} \min \frac{J^{(3)}(\tilde{h})}{(k\theta)(\tau\theta)}, \quad (29)$$

$$Q_T = \frac{2}{\delta^2} \min \frac{J^{(2)}(\tilde{h})}{(\tau\theta)^2}. \quad (30)$$

3. Derivation of the Slip Coefficients and the Thermal Molecular Pressure Exponent

Over the last decades, the application of the Boltzmann equation to describe flows in nano- and microfluidic devices has become an area of intense research. Unfortunately, when applied to realistic multidimensional problems, the numerical solution of the kinetic equations is computationally demanding. However, in the case of low rarefaction level, the gas flow can be still simulated in the frame of the classical hydrodynamic (Navier–Stokes) equations, provided that slip boundary conditions are employed. These conditions involve slip parameters which depend on the gas-surface interaction potential through the accommodation coefficients. In particular, in the frame of the Cercignani-Lampis boundary conditions, α_t and α_n describe the tangential momentum and normal energy exchange at the solid-gas interfaces, respectively. This heat and momentum transfer highly affects the thermo-physical properties of a gas. Therefore, to improve our understanding of the gas-surface interaction to be used in practical applications, it is useful to derive a general method for extracting the accommodation coefficients, regardless of the driving mechanism of the fluid flow.

For pressure-driven flows, assuming a first-order boundary condition at a flat wall, in the isothermal case, the slip velocity reads as

$$v_s = \sigma_p^{(1)} \lambda \left(\frac{\partial v}{\partial x} \right)_w, \quad (31)$$

where $\sigma_p^{(1)}$ is the viscous-slip coefficient, λ is the mean free path of the molecules and the gas-velocity gradient is evaluated at the wall. Likewise, for thermal-driven flows, one can write the following first-order slip boundary condition on a flat wall:

$$v_s = \sigma_T^{(1)} \frac{\mu}{\rho T} \left(\frac{\partial T}{\partial z} \right)_w, \tag{32}$$

where $\sigma_T^{(1)}$ is the thermal slip coefficient, μ is the gas viscosity, and the temperature gradient is evaluated at the wall. The asymptotic near-continuum solutions of the Boltzmann equation for the Poiseuille and thermal-creep flows allow one to indirectly compute both the viscous and thermal slip coefficients, respectively. Equations (28) and (29) give in the limit $\delta \gg 1$:

$$G_p = \frac{\delta}{\sigma_{0,p}} + \sigma_{1,p} + \frac{\sigma_{2,p}}{\delta} + \cdots \tag{33}$$

$$G_T = \frac{\sigma_{1,T}}{\delta} + \frac{\sigma_{2,T}}{\delta^2} + \cdots \tag{34}$$

where

$$\sigma_{0,p} = (4\sqrt{\pi})^{-1} \cdot \left[\frac{96}{\pi} \hat{J}_1 + 48\sqrt{\pi} \right], \quad \sigma_{1,p} = [4\sqrt{\pi}\alpha_t \mathcal{A}_p]^{-1} \cdot [\mathcal{D}_p - 16/9\pi\alpha_t \mathcal{C}_p], \tag{35}$$

$$\sigma_{2,p} = [4\sqrt{\pi}\alpha_t \mathcal{A}_p]^{-1} \cdot [\mathcal{E}_p + 16/9\pi\alpha_t \mathcal{C}_p^2 - 16/9\pi\alpha_t \mathcal{B}_p - \mathcal{C}_p \mathcal{D}_p] \tag{36}$$

$$\mathcal{A}_p = \frac{32}{3\pi} \hat{J}_1 + \frac{16}{3}\sqrt{\pi}, \quad \mathcal{D}_p = \frac{128}{3} \hat{J}_1 - \frac{32}{3}\pi^{3/2}\alpha_t + \frac{64}{3}\pi^{3/2}, \tag{37}$$

$$\mathcal{B}_p = \mathcal{A}_p^{-1} \cdot \left[\frac{128}{\pi} \hat{J}_2 - 16\sqrt{\pi}\alpha_t - 16\sqrt{\pi}\alpha_n + 16\sqrt{\pi}\alpha_t\alpha_n \right], \tag{38}$$

$$\mathcal{C}_p = \mathcal{A}_p^{-1} \cdot [-16 - 4\pi\alpha_t - 64\mathcal{F}_0\alpha_n(1-\alpha_t) - 64\mathcal{F}_1(1-\alpha_t)(1-\alpha_n)], \tag{39}$$

$$\mathcal{E}_p = -64\pi + \frac{64}{3}\pi\alpha_t - 256\pi\mathcal{F}_0\alpha_n(1-\alpha_t) - 256\pi\mathcal{F}_1(1-\alpha_t)(1-\alpha_n) \tag{40}$$

and

$$\sigma_{1,T} = \left[64\hat{J}_4 \left(\frac{2\hat{J}_1}{\pi^{3/2}} + 1 \right) \right]^{-1} \left[16\left(5\hat{J}_1 - 10\hat{J}_3 + 2\hat{J}_4 \right) + 10\,\pi^{3/2} \left(\alpha_t + \alpha_n - \alpha_t\alpha_n + 4 \right) \right], \tag{41}$$

$$\sigma_{2,T} = [2\sqrt{\pi}\mathcal{A}_T]^{-1} \left[\frac{\mathcal{B}_T \mathcal{C}_T}{\mathcal{A}_T} - \mathcal{E}_T \right], \quad \mathcal{A}_T = \frac{32\,\hat{J}_4\,\alpha_t}{3\sqrt{\pi}} \left[\frac{2\hat{J}_1}{\pi^{3/2}} + 1 \right], \tag{42}$$

$$\begin{aligned} \mathcal{B}_T \;&= -\frac{128}{\pi}\hat{J}_4\alpha_t(1-\alpha_t)\left[\mathcal{F}_0\alpha_n + \mathcal{F}_1(1-\alpha_n) \right] - 8\alpha_t\hat{J}_4\left[\frac{4}{\pi} + \alpha_t \right] \\ &\quad + \frac{16}{3}\sqrt{\pi}\alpha_t \left[\alpha_n + 7\,\alpha_t + 2\,\alpha_t^3 - 6\,\alpha_t^2 - \alpha_t\,\alpha_n \right] \left[\frac{2\hat{J}_1}{\pi^{3/2}} + 1 \right], \end{aligned} \tag{43}$$

$$\mathcal{C}_T = -\frac{16}{3}\alpha_t \left[5\,\hat{J}_1 - 10\,\hat{J}_3 + 2\,\hat{J}_4 \right] - \frac{10}{3}\pi^{3/2}\alpha_t \left[\alpha_t + \alpha_n - \alpha_t\,\alpha_n + 4 \right], \tag{44}$$

$$\begin{aligned} \mathcal{E}_T \;&= -32\sqrt{\pi}\alpha_t \left[5\,\hat{J}_3 - \hat{J}_4 \right] + 160\pi\alpha_t(1-\alpha_t)\left[\mathcal{F}_0\alpha_n + \mathcal{F}_1(1-\alpha_n) \right] + 10\pi^2\alpha_t \\ &\quad \times \left[2\,\alpha_t + \alpha_n - \alpha_t\,\alpha_n \right] - \frac{32}{3}\pi\alpha_t \left[\alpha_t - 2\,\alpha_n - 3\,\alpha_t^2 + \alpha_t^3 + 2\,\alpha_t\,\alpha_n - \frac{15}{4} \right], \end{aligned} \tag{45}$$

with $\hat{J}_1 = -1.4180$, $\hat{J}_2 = 1.8909$, $\hat{J}_3 = 0.9449$, $\hat{J}_4 = 4.7252$, $\mathcal{F}_0 = 0.196079$ and $\mathcal{F}_1 = 0.247679$. The definition of the integral expressions $\hat{J}_i$ is reported in the Appendix A. The reliability of a "second-order" solution for the pressure- and temperature-driven mass flow rate (Equations (33) and (34)) has been well assessed in Refs. [31,40,41].

If one compares the thermal-driven mass flow rate obtained by using the Navier–Stokes equations with the slip boundary conditions (32) and the variational formula (34), it is straightforward to identify $\sigma_{1,T}$ with the first-order thermal slip coefficient $\sigma_T^{(1)}$, while $\sigma_{2,T}$ can be referred to as the "second-order" thermal slip coefficient (where we indicate with "second-order" a term of the next-order with respect to the leading one). Likewise, this identification can be performed for the Poiseuille flow (a complete derivation is presented in Refs. [40,41]). Furthermore, the formulas (33) and (34) can be used to theoretically calculate the γ-exponent. Assuming that the pressure and temperature drops are small, one can integrate Equation (17) along the longitudinal direction z to obtain:

$$\gamma = \frac{G_T}{G_p}. \tag{46}$$

4. Experimental Measurements

The measurements of the thermal molecular pressure difference and the temperature driven mass flow rates have been made by various authors and some of these works have been cited in Section 1. The authors of Ref. [29] provided a set of data on the TPD and also on the TPE. They found that the γ-exponent can vary with the gas nature and the gas rarefaction, from 0 in the hydrodynamic flow regime to 0.5 in the free molecular one. Recently, a series of measurements of the temperature driven flows have been carried out [42–44] in the capillary glass tube with radius of 0.245 mm for three temperature differences, 37 °C, 53.5 °C and 71 °C, keeping the cold temperature around 27 °C. The TPD, TPR and γ values are provided for helium, argon and nitrogen.

The authors of Refs. [32,45] measured the different characteristics of the temperature driven mass flow rate through a microchannel over a wide range of the gas rarefaction parameter using the same experimental apparatus. A microchannel made of PEEK (PolyEtherEtherKetone) has been employed with a rectangular cross-section and the following dimensions: a height of $d = 0.22 \pm 0.01$ mm, a width of $w = 6$ mm, and a length of $L = 73$ mm. The temperature of the hot reservoir T_h and that of the cold reservoir T_c were maintained constant and two temperature differences ΔT have been tested: (1) $T_\mathrm{h} = 347.1 \pm 0.5$ K, $T_\mathrm{c} = 289.2 \pm 0.2$ K, where $\Delta T = 57.9$ K and (2) $T_\mathrm{h} = 337.0 \pm 0.6$ K, $T_\mathrm{c} = 299.6 \pm 0.4$ K, where $\Delta T = 37.4$ K. Such temperature differences were chosen to have the same mean temperature $T_\mathrm{m} = (T_\mathrm{c} + T_\mathrm{h})/2 = 318$ K. The final equilibrium flow characteristics, as the thermal molecular pressure difference, the thermal molecular pressure ratio and the thermal molecular pressure exponent, were evaluated as functions of the rarefaction parameter from the measurements of pressure variations in time in both hot and cold reservoirs. The thermal molecular pressure difference has been measured for 5 noble gases (helium, neon, argon, krypton and xenon) and for polyatomic nitrogen.

The measurements of the thermal-creep mass flow rates have been reported in Ref. [32]. In this case, only the second term on the right-hand side of Equation (17) has been taken into account, modified as follows in order to consider a rectangular channel of width w:

$$\dot{M}_\mathrm{T} = \frac{d^2\, p\, w\, G_T}{\sqrt{2RT}}\, \frac{1}{T}\frac{dT}{dz}. \tag{47}$$

The lateral-wall effects have been neglected owing to the large channel width-to-height ratio equal to 27.3 [46,47]. Thus, the dimensionless thermal-creep coefficient G_T for a gas flowing between two parallel infinite plates at a distance d apart can be used. In Equation (47), G_T depends on the local rarefaction parameter δ. Indeed, in the experiments,

the variation of δ along the channel is small enough to approximate $G_T(\delta)$ by $G_T(\delta_\mathrm{m})$, where the mean rarefaction parameter δ_m is calculated on the basis of the mean temperature T_m:

$$\delta_\mathrm{m} = \frac{p\,d}{\mu(T_\mathrm{m})\sqrt{2RT_\mathrm{m}}}. \tag{48}$$

The viscosity coefficient is computed using the following relation [48]:

$$\mu = \mu_\mathrm{ref}\left(\frac{T}{T_\mathrm{ref}}\right)^{\omega} \tag{49}$$

where μ_ref is the viscosity coefficient at the temperature T_ref and ω is the viscosity index.

The experimental values for G_T as a function of δ_m have been listed in Ref. [32] (Table 1), for different noble gases. To extract the first- and second-order slip coefficients from the experiments and mostly to improve the accuracy in evaluating the first order coefficient, Equation (47) has been used with G_T given by its asymptotic expression (34):

$$G_T \simeq \frac{\sigma_{1,T}^\mathrm{exp}}{\delta} + \frac{\sigma_{2,T}^\mathrm{exp}}{\delta^2}. \tag{50}$$

In Equation (50), we renamed the two coefficients $\sigma_{1,T}$ and $\sigma_{2,T}$, appearing in (34), with $\sigma_{1,T}^\mathrm{exp}$ and $\sigma_{2,T}^\mathrm{exp}$ to highlight that the latter are experimentally-determined coefficients. Integrating the resulting expression along the channel (by using the property of mass conservation) with μ given by (49) and δ substituted by its mean value δ_m (48), one obtains:

$$\dot{M}_\mathrm{T} = \dot{M}_\mathrm{ref}\left[\sigma_{1,T}^\mathrm{exp} + \frac{\sigma_{2,T}^\mathrm{exp}}{\delta_\mathrm{m}}\sigma + \mathcal{O}\left(\frac{1}{\delta_\mathrm{m}^2}\right)\right] \tag{51}$$

where $\dot{M}_\mathrm{ref}$ reads

$$\dot{M}_\mathrm{ref} = \frac{d\,w\,\mu_\mathrm{ref}}{T_\mathrm{ref}^\omega}\frac{(T_\mathrm{h}^\omega - T_\mathrm{c}^\omega)}{\omega\,L}. \tag{52}$$

Since the constant σ in Equation (51) has been found to be quite close to unity, one can fit the measured data on the mass flow rate with the formula:

$$\frac{\dot{M}_\mathrm{T}}{\dot{M}_\mathrm{ref}} = \sigma_{1,T}^\mathrm{exp} + \frac{\sigma_{2,T}^\mathrm{exp}}{\delta_\mathrm{m}}. \tag{53}$$

The fitting procedure has been carried out in the range of $\delta_\mathrm{m} = [3, 40]$, since the asymptotic formula (51) allows one to predict the mass flow rate also in the early transition regime. The validity of this interval has been already assessed in [31], on the basis of theoretical computations. The values of $\sigma_{1,T}^\mathrm{exp}$ and $\sigma_{2,T}^\mathrm{exp}$ are listed in Ref. [32] (Table 3), for both $\Delta T = 57.9\,\mathrm{K}$ and $\Delta T = 37.4\,\mathrm{K}$, and for five different noble gases: helium (He), neon (Ne), argon (Ar), krypton (Kr) and xenon (Xe). In Ref. [45] the information on the γ-exponent (Equation (2)) is obtained from the steady state flow condition, i.e., when the thermal creep flow in the channel is counterbalanced by the Poiseuille flow generated by a pressure difference between the tanks. Therefore, this quantity is influenced not only by the temperature driven flow but also by the pressure driven one. It is worthwhile to note that experimentally-obtained values of γ are essentially lower than 0.5.

5. Results and Discussion

The present investigation is mostly guided by the desire to analyze recent experimental studies, described in detail in Section 4, in order to propose a reliable procedure of extraction for the tangential momentum and normal energy accommodation coefficients. In Ref. [32] the thermal slip coefficients $\sigma_{1,T}$ and $\sigma_{2,T}$ have been obtained applying a fitting procedure to mass flow rate measurements. In Table 1, we listed the experimental estimates of $\sigma_{1,T}$

and $\sigma_{2,T}$ for each $\Delta T = 58$ K and $\Delta T = 37$ K, and also the experimental estimates using the data for the two temperature differences (indicated by 'All').

Table 1. Experimental estimates for the first-($\sigma_{1,T}$) and second-order ($\sigma_{2,T}$) thermal slip coefficients (with permission of [32]).

	All		$\Delta T = 58$ **K**		$\Delta T = 37$ **K**	
	$\sigma_{1,T}^{\mathrm{exp}}$	$\sigma_{2,T}^{\mathrm{exp}}$	$\sigma_{1,T}^{\mathrm{exp}}$	$\sigma_{2,T}^{\mathrm{exp}}$	$\sigma_{1,T}^{\mathrm{exp}}$	$\sigma_{2,T}^{\mathrm{exp}}$
He	1.006 ± 0.020	-1.147 ± 0.113	1.026 ± 0.027	-1.196 ± 0.149	0.985 ± 0.023	-1.100 ± 0.127
Ne	0.998 ± 0.029	-1.226 ± 0.172	1.013 ± 0.025	-1.197 ± 0.147	0.983 ± 0.049	-1.255 ± 0.290
Ar	1.017 ± 0.057	-1.274 ± 0.406	1.038 ± 0.035	-1.248 ± 0.249	0.997 ± 0.105	-1.299 ± 0.763
Kr	1.061 ± 0.053	-1.327 ± 0.400	1.111 ± 0.076	-1.442 ± 0.566	1.012 ± 0.074	-1.212 ± 0.554
Xe	1.102 ± 0.085	-1.746 ± 0.626	1.142 ± 0.087	-1.547 ± 0.640	1.061 ± 0.142	-1.946 ± 1.050

In the previous paper [31], relying on a numerical solution of the system (41) and (42), where on the left-hand side we used values of $\sigma_{1,T}$ and $\sigma_{2,T}$ as close as possible to the experimental measurements, we extracted a pair of accommodation coefficients α_t, α_n, for each noble gas considered in the experiments: helium, neon, argon, krypton and xenon. Although the system (41) and (42) is highly nonlinear in the unknowns α_t and α_n, we numerically found only one solution for each fixed $\sigma_{1,T}$ and $\sigma_{2,T}$. Indeed, a recent deeper inspection, carried out analytically by means of symbolic tools, has revealed that for some specific values of the thermal-slip coefficients, there can exist multiple solutions for the accommodation coefficients. This means that, we can derive the same values of $\sigma_{1,T}$ and $\sigma_{2,T}$, with α_t and α_n ranging within a continuous interval and obtain equally accurate temperature-driven mass flow rates. Therefore, if one relies only on the experimental data presented in [32], there is no way to uniquely determine α_t and α_n.

To overcome this difficulty, we took into account a further series of measurements, carried out with the same experimental apparatus of Ref. [32], where the thermal molecular pressure exponent γ has been evaluated [45]. Since we verified that γ mostly depends on the accommodation coefficient of the tangential momentum, the parameter α_t has been fixed first by comparing our variational results based on Equations (33), (34) and (46), with the experimental data of γ (reported in [45]). Then α_n has been chosen accordingly in order to obtain thermal slip coefficients as close as possible to the experimental measurements (reported in [32]). We have listed in Table 2 these variational-determined thermal slip coefficients, $\sigma_{1,T}$ and $\sigma_{2,T}$, along with the specific values of α_t and α_n extracted in order to optimize the agreement between the theoretical results and the measurements performed in both experiments [32,45]. The comparison between the variational calculations (formulas (33), (34) and (46)) and the experimental data showing the dimensionless thermal-creep mass flow rate G_T and the γ-exponent is drawn in Figures 1–10.

Table 2. Variational predictions for the first-($\sigma_{1,T}$) and second-order ($\sigma_{2,T}$) thermal slip coefficients along with the accommodation coefficients (α_t, α_n), chosen to provide results as close as possible to the experimental measurements.

	$\sigma_{1,T}$	$\sigma_{2,T}$	α_t	α_n
He	1.0480	−1.1324	0.63	0.54
Ne	1.0548	−1.1669	0.60	0.62
Ar	1.0661	−1.2249	0.63	0.67
Kr	1.0817	−1.3067	0.65	0.77
Xe	1.1119	−1.4693	0.70	1.00

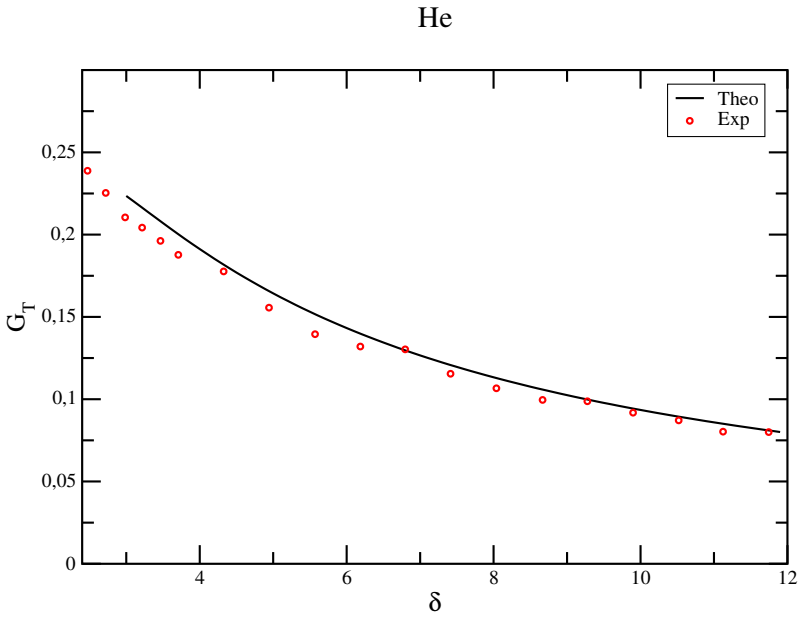

Figure 1. Comparison between the measured mass flow rate G_T of helium for $\Delta T = 58$ K (Exp) and our variational outputs (Theo) with $\alpha_t = 0.63$ and $\alpha_n = 0.54$.

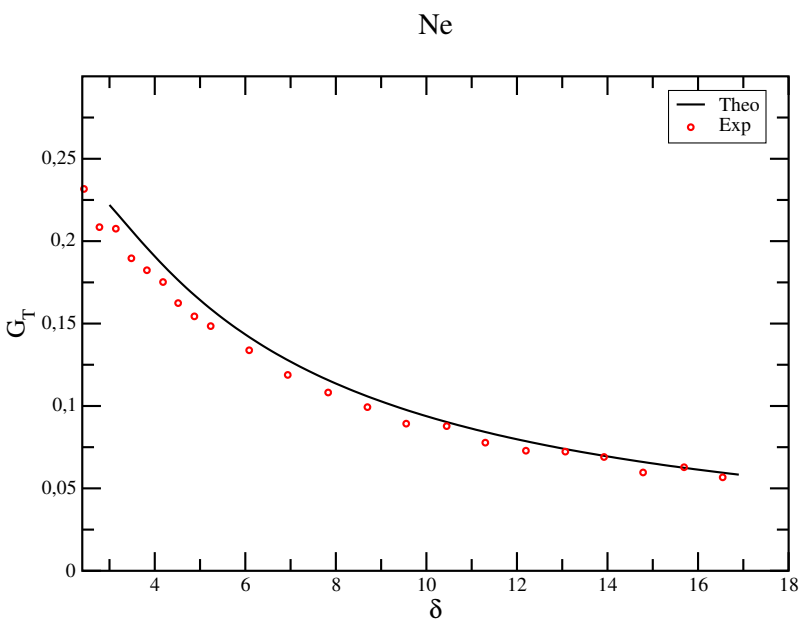

Figure 2. Comparison between the measured mass flow rate G_T of neon for $\Delta T = 58$ K (Exp) and our variational outputs (Theo) with $\alpha_t = 0.6$ and $\alpha_n = 0.62$.

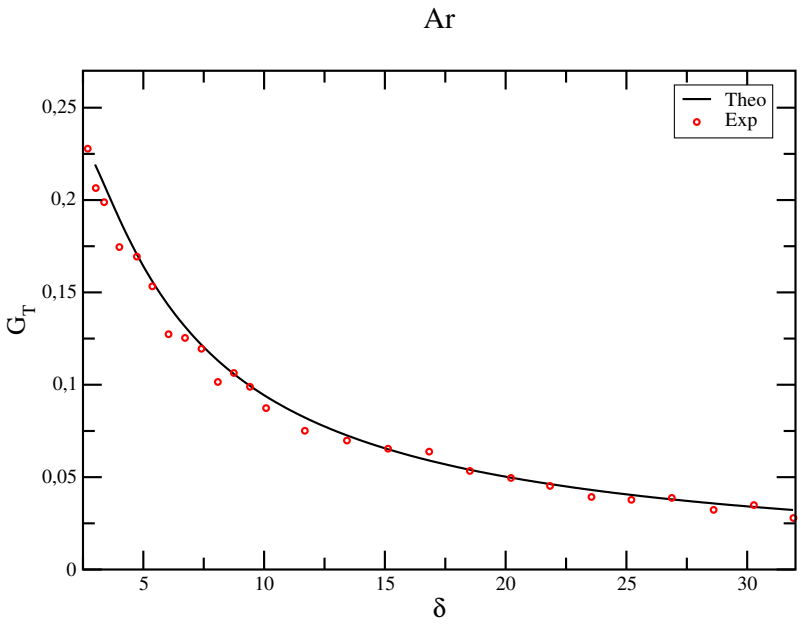

Figure 3. Comparison between the measured mass flow rate G_T of argon for $\Delta T = 58$ K (Exp) and our variational outputs (Theo) with $\alpha_t = 0.63$ and $\alpha_n = 0.67$.

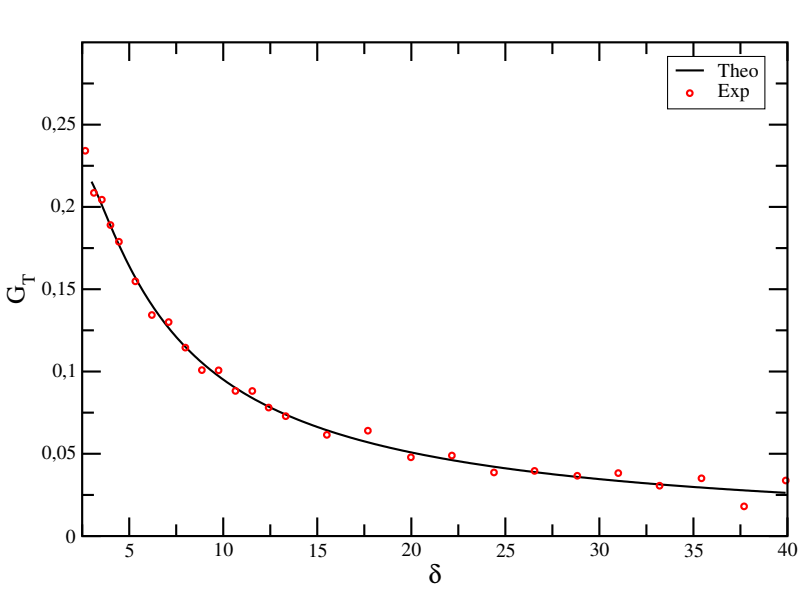

Figure 4. Comparison between the measured mass flow rate G_T of krypton for $\Delta T = 58$ K (Exp) and our variational outputs (Theo) with $\alpha_t = 0.65$ and $\alpha_n = 0.77$.

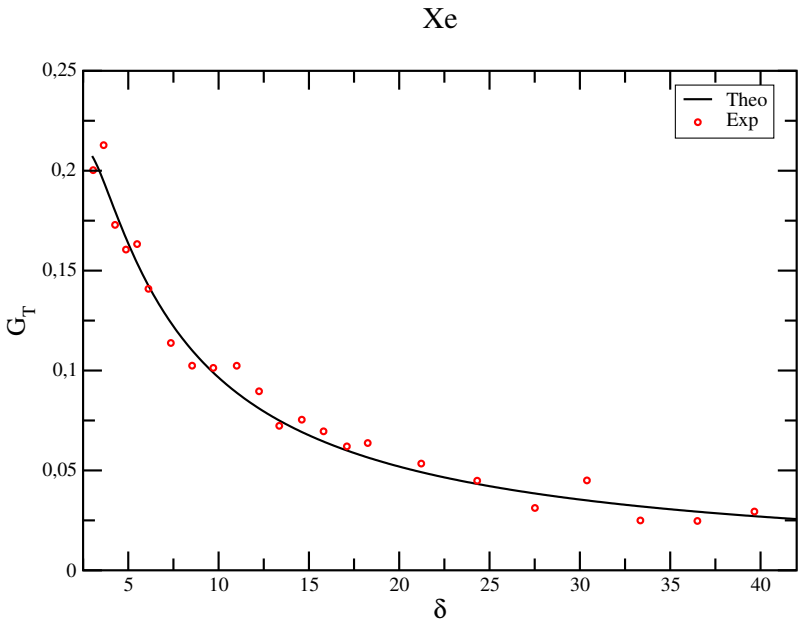

Figure 5. Comparison between the measured mass flow rate G_T of xenon for $\Delta T = 58$ K (Exp) and our variational outputs (Theo) with $\alpha_t = 0.7$ and $\alpha_n = 1$.

In these pictures, we reported only the results of the experiments performed with a temperature difference between the hot and cold reservoir equal to $\Delta T = 58$ K. The agreement with the measurements obtained when $\Delta T = 37$ K is fairly good for most of the gases used in the experiments. However, there are some cases (as for xenon) where the experimental data for $\Delta T = 37$ K are more scattered, and this produces a discrepancy between the measured quantities (see, for instance, the value of $\sigma_{2,T}$ for xenon in Table 1) and finally less good agreement with modeling. Indeed, the measured pressure variation, induced by the thermal creep flow, is smaller for heavier gas species (like xenon) and for small temperature differences, leading to a relatively larger measurement error.

Comparing the values of the first- and second-order thermal slip coefficients reported in Table 2 of the present paper with those listed in Table II of Ref. [31], one can immediately recognize that these coefficients have remained unchanged for four gases (helium, neon, argon, krypton). However, still the associated accommodation coefficients (α_t, α_n) are different, since in Ref. [31] the authors have compared the variational results with a set of experimental data related only to the thermal-creep mass flow rate G_T, while in the present paper the agreement with the measured thermal molecular pressure exponent γ is also evaluated. Owing to the existence of multiple pairs of accommodation coefficients (α_t, α_n), solutions of the system (41) and (42), we were able to leave unchanged $\sigma_{1,T}$ and $\sigma_{2,T}$, which have already given rise to a good agreement between experimental and theoretical results for G_T [31], and we chose the most appropriate accommodation coefficients in order to reproduce also the measured values of γ. This procedure has been proven to be effective for all gases except xenon. The problem with xenon is that the experimental data for γ can only be accurately reproduced (in both cases when $\Delta T = 58$ K and $\Delta T = 37$ K) if $\alpha_t \simeq 0.7$, while a so strongly negative second-order thermal slip coefficient, as measured in the experiments with a temperature difference $\Delta T = 37$ K, is compatible only with $\alpha_t > 1$. Therefore, unlike what has been done in [31], in this work we took into account only the experiments with $\Delta T = 58$ K (which provide less scattered data) and accordingly, for xenon, we reported in Table 2 the variational-determined values of $\sigma_{1,T}$ and $\sigma_{2,T}$ which better reproduce only this kind of measurements.

For the comparison between the theoretical and experimental results shown in Figures 1–10, we adopted the conventional approach by defining a mean free path through the classical hard sphere model, [49,50]:

$$\lambda = \frac{\sqrt{\pi}}{2}\frac{\mu}{p}\sqrt{2RT}. \tag{54}$$

To derive Equation (54) it has been assumed that $\mu \propto T^{1/2}$ while the real gas coefficient of viscosity μ is proportional to T^{ω}. A way to overcome this difficulty is to use Equation (54) along with the definition (49) for the coefficient of viscosity. An alternative route to define a consistent mean free path has been proposed a long time ago by Bird [48], who introduced the variable cross-section hard sphere (VHS) model. This model properly accounts for the real gas temperature exponent of the coefficient of viscosity. Indeed, our variational results have been obtained for a hard-sphere gas, therefore we use Equation (54) also to represent the experimental data. Accordingly, the rarefaction parameter δ appearing in Figures 1–10 reads:

$$\delta = \frac{pd}{\mu\sqrt{2RT}}, \tag{55}$$

where the viscosity μ is given by Equation (49), so the values of δ reported in Equations (48) and (55) coincide. In Figures 1–10, the interval of variation for the rarefaction parameter is different for each gas since in the experiments the pressure range has been taken to be the same, while the viscosity and the most probable velocity of each species are different.

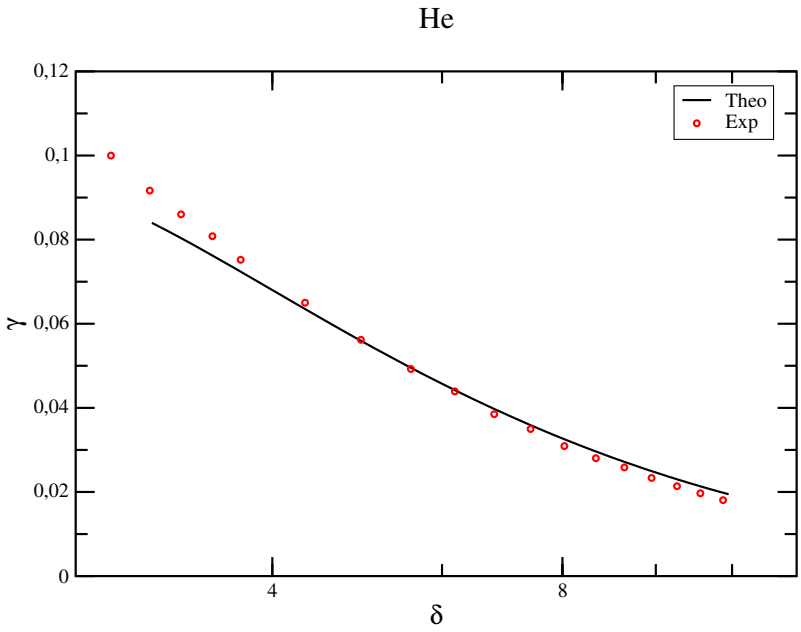

Figure 6. Comparison between the measured thermal molecular pressure exponent (γ) of helium for $\Delta T = 58$ K (Exp) and our variational outputs (Theo) with $\alpha_t = 0.63$ and $\alpha_n = 0.54$.

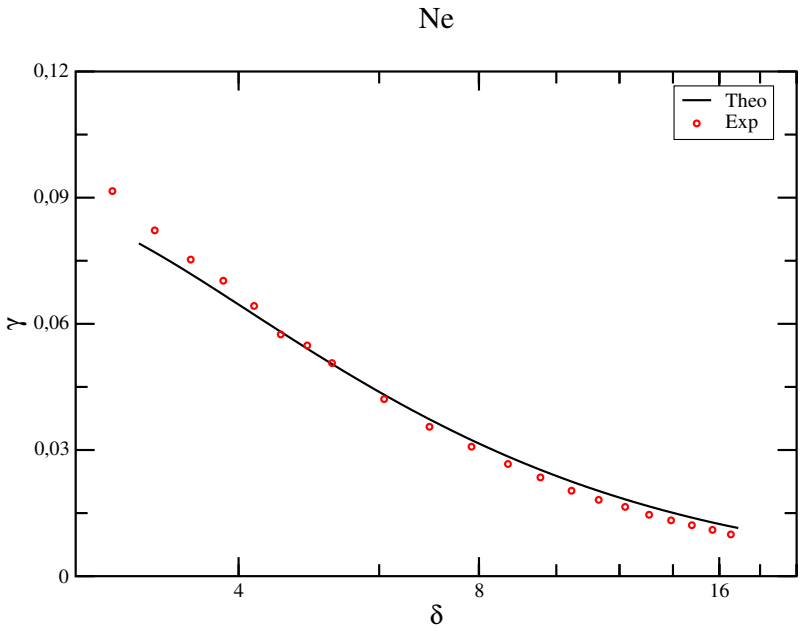

Figure 7. Comparison between the measured thermal molecular pressure exponent (γ) of neon for $\Delta T = 58$ K (Exp) and our variational outputs (Theo) with $\alpha_t = 0.6$ and $\alpha_n = 0.62$.

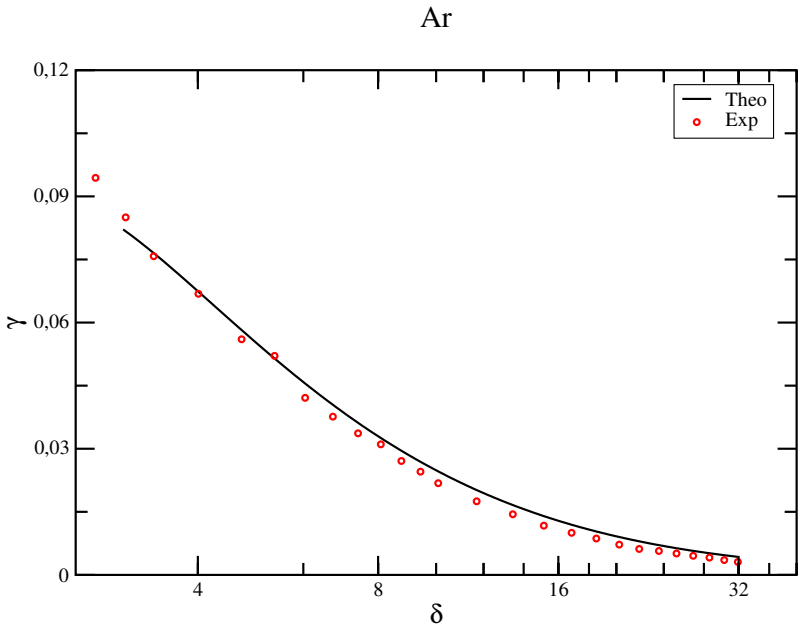

Figure 8. Comparison between the measured thermal molecular pressure exponent (γ) of argon for $\Delta T = 58$ K (Exp) and our variational outputs (Theo) with $\alpha_t = 0.63$ and $\alpha_n = 0.67$.

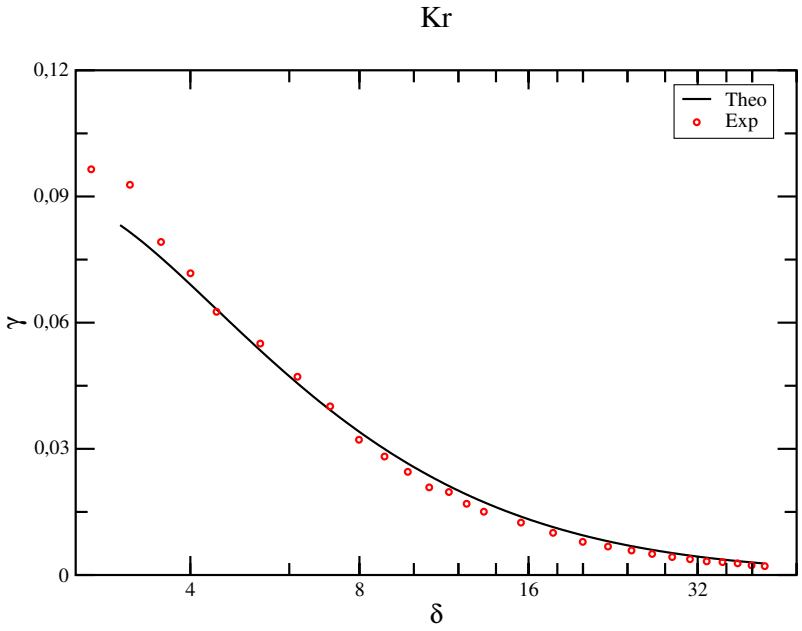

Figure 9. Comparison between the measured thermal molecular pressure exponent (γ) of krypton for $\Delta T = 58$ K (Exp) and our variational outputs (Theo) with $\alpha_t = 0.65$ and $\alpha_n = 0.77$.

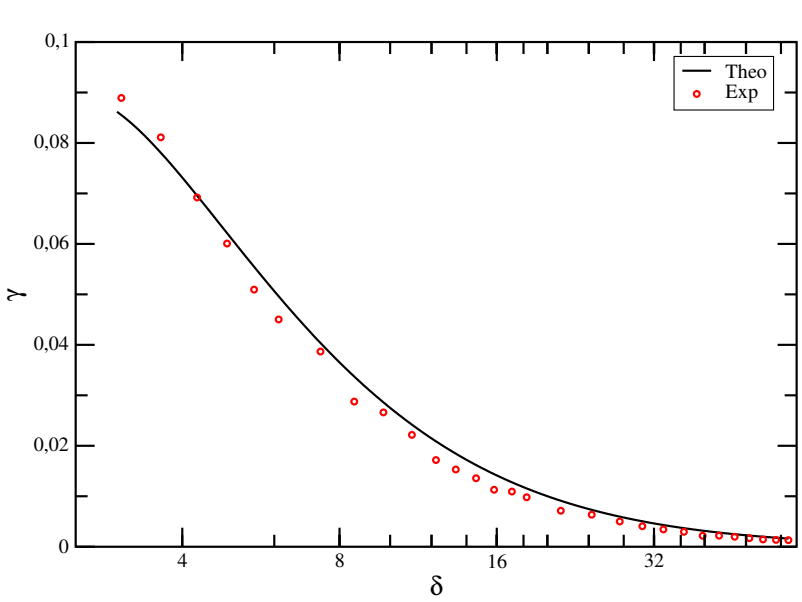

Figure 10. Comparison between the measured thermal molecular pressure exponent (γ) of xenon for $\Delta T = 58$ K (Exp) and our variational outputs (Theo) with $\alpha_t = 0.7$ and $\alpha_n = 1$.

6. Concluding Remarks

In the present study, a variational technique applied to the Boltzmann equation for hard-sphere molecules has been used to derive analytical expressions for the first- and second-order thermal slip coefficients in terms of the tangential momentum and the normal energy accommodation coefficients, defined in the frame of the Cercignani-Lampis model of boundary conditions. A new method for extracting the accommodation coefficients has been proposed by comparing the theoretical results with two series of measurements carried out with the same experimental apparatus, where the channel surfaces are made of PEEK [32,45]. Since the thermal molecular pressure exponent mainly depends on α_t, we fixed the tangential momentum accommodation coefficient by requiring a fair agreement with the experimental measurement of γ, given in [45]. Then, among the multiple pairs

of variational solutions for (α_t, α_n), leading to the same first- and second-order thermal slip coefficients, chosen to closely approximate the experimental data reported in [32], we selected the unique pair with the previously determined value of α_t. The mathematical constraint that both thermal creep and Poiseuille flows are needed to fully derive in a consistent way the parameters (α_t, α_n) has a physical counterpart, in that these problems are strongly related to each other: when a temperature gradient exists along the channel walls, then a thermal transpiration flow is induced from the cold side towards the hot side of the channel and this produces a pressure-driven backflow. In addition, since the analytical formulas derived from our variational method are valid for $\delta \gtrsim 3$ and the data are provided for $\delta = [3, 40]$, the fitting procedure between the theoretical and experimental results has been carried out in a wide range of the rarefaction parameter. The values of the accommodation coefficients (α_t, α_n) extracted in our work are consistent with those recently reported in [30] for argon, while a significant deviation (especially related to the value of α_n) is highlighted for helium. Indeed, by analyzing the data reported in [32,45] it is not possible to detect a significant discrepancy in the measured quantities for the different gases (in particular, about the first- and second-order thermal slip coefficients) such as to justify a remarkable difference in the values of the accommodation coefficients between the helium and the other gases. Since the accommodation coefficients strongly depend on the properties of both the gas and the solid surface on which a molecule impinges, part of our future research should focus on extending the variational method in order to take into account interaction potentials more realistic than the hard-sphere model. In fact, if one considers, for instance, the viscosity index ω, gases like argon, krypton and xenon show significant deviations from a hard-sphere gas behaviour. On the other hand, new experimental measurements are desirable to inspect more deeply the influence of the walls material of the microchannel, also allowing for a more straightforward comparison with the data available in the literature.

Author Contributions: Methodology, S.L.; software, T.M. and S.L.; validation, S.L. and T.M.; investigation, S.L.; data curation, H.Y.; writing—original draft preparation, S.L. and I.G.; writing—review and editing, S.L., I.G. and H.Y.; visualization, S.L. and H.Y.; supervision, S.L. All authors have read and agreed to the published version of the manuscript.

Funding: This research received no external funding.

Institutional Review Board Statement: Not applicable.

Informed Consent Statement: Not applicable.

Data Availability Statement: The data presented in this study are available in the displayed figures and tables within the article but can also be obtained on request from the corresponding author within a reasonable time-frame.

Acknowledgments: S.L. was supported by the GNFM of INdAM (Istituto Nazionale di Alta Matematica "F. Severi"), Italy.

Conflicts of Interest: The authors declare no conflict of interest.

Appendix A

In Equations (35)–(45), the symbol $\hat{J}_i$ stands for integral expressions defined by using the brackets $[\phi, \psi]$,

$$[\phi, \psi] = \int_{-\infty}^{+\infty} \int_{-\infty}^{+\infty} \int_{-\infty}^{+\infty} e^{-c^2} \phi(c) L\psi \, d\mathbf{c}, \tag{A1}$$

with $L\psi$ being the linearized Boltzmann collision operator. For hard spheres of diameter σ, the mean free path λ reads as $\lambda = 1/(\sqrt{2}\pi\sigma^2 n)$ (where n is the number density). Therefore,

$$L\psi = \frac{1}{4\sqrt{2}\pi^{5/2}\lambda} \int_0^{2\pi} d\epsilon \int_0^{\pi} \sin\Theta d\Theta \cdot \int_{-\infty}^{+\infty} e^{-{c_1}^2} V \left(\psi_1' + \psi' - \psi_1 - \psi\right) d\mathbf{c_1}, \tag{A2}$$

where ψ is a function of $\mathbf{c}$, while ψ_1 refers to $\mathbf{c_1}$. V is the relative velocity: $|\mathbf{c} - \mathbf{c_1}|$. $\psi' \equiv \psi(\mathbf{c}')$ and $\psi'_1 \equiv \psi(\mathbf{c}'_1)$, where $\mathbf{c}'$ and $\mathbf{c}'_1$ are the velocities after collision of two molecules with velocities $\mathbf{c}$ and $\mathbf{c_1}$, respectively. The collision geometry, in conjunction with the conservation laws, relates the velocities after collision to the velocities before collision. Thus,

$$c'_x = c_x + (c_{1x} - c_x)\cos^2(\Theta/2) + 1/2 \cdot [V^2 - (c_{1x} - c_x)^2]^{1/2}\sin\Theta\cos\epsilon,$$
$$c'_{1x} = c_{1x} - (c_{1x} - c_x)\cos^2(\Theta/2) - 1/2 \cdot [V^2 - (c_{1x} - c_x)^2]^{1/2}\sin\Theta\cos\epsilon,$$

where Θ is the angle through which the relative velocity has turned and ϵ is the azimuthal angle that the plane containing the relative velocities before and after collision makes with a fixed reference plane. Similar relations exist for the y and z components [48].

The integrals J_1, J_2, J_3, J_4 appearing in Equations (35)–(45) are eightfold integrals,

$$J_1 = [c_x c_z, c_x c_z], \quad J_2 = -[{c_x}^2 c_z, c_x {c_z}^2]$$
$$J_3 = -[{c_x}^2 c_z, c^2 c_z], \quad J_4 = -[c^2 c_z, c^2 c_z], \tag{A3}$$

where $\hat{J}_i = \frac{2\lambda}{\sqrt{\pi}} J_i$. These integrals have been computed using a Monte Carlo integration on an eight-dimensional space. In order to validate this numerical scheme, we recalculated with the Monte Carlo method the collision integrals evaluated in Refs. [51,52], by means of the analytical technique developed by Wang Chang and Uhlenbeck [53].

References

1. Reynolds, O. On certain Dimensional properties of Matter in the gaseous state. *Philos. Trans. R. Soc. Lond.* **1879**, *170*, 727–845.
2. Maxwell, J.C. On stress in rarefied gases arising from inequalities of temperature. *Phil. Trans. R. Soc. Lond.* **1879**, *170*, 231–256.
3. Knudsen, M. Eine Revision der Gleichgewichtsbedingung der Gase. Thermische Mlekularstömung. *Ann. Der Phys.* **1910**, *31*, 205–229.
4. Knudsen, M. Thermischer Molekulardruck der Gase in Röhern. *Ann. Der Phys.* **1910**, *33*, 1435–1448. [CrossRef]
5. Martini, V.; Bernardini, S.; Bendahan, M.; Aguir, K.; Perrier, P.; Graur, I. Microfluidic gas sensor with integrated pumping system. *Sens. Actuators B Chem.* **2012**, *170*, 45–50. [CrossRef]
6. Martini-Laithier, V.; Graur, I.; Bernardini, S.; Aguir, K.; Perrier, P.; Bendahan, M. Ammonia detection by a novel Pyrex microsystem based on thermal creep phenomenon. *Sens. Actuators B Chem.* **2014**, *192*, 714–719. [CrossRef]
7. Vargo, S.E.; Muntz, E.P. Initial results from the first MEMS fabricated thermal transpiration-driven vacuum pump. In Proceedings of the AIP Conference Proceedings. AIP, AIP RAREFIED GAS DYNAMICS: 22nd International Symposium, Sydney, Australia, 9–14 July 2000; Volume 585, pp. 502–509. [CrossRef]
8. Alexeenko, A.A.; Fedosov, D.A.; Gimelshein, S.F.; Levin, D.A.; Collins, R.J. Transient Heat Transfer and Gas Flow in a MEMS-Based Thruster. *J. Microelectromech. Syst.* **2006**, *15*, 181–194. [CrossRef]
9. Han, Y.L.; Muntz, E.P.; Alexeenko, A.; Young, M. Experimental and Computational Studies of Temperature Gradient–Driven Molecular Transport in Gas Flows through Nano/Microscale Channels. *Nanoscale Microscale Thermophys. Eng.* **2007**, *11*, 151–175. [CrossRef]
10. Quesada, G.L.; Giorgos Tatsios, G.; Valougeorgis, D.; Rojas-Cárdenas, M.; Baldas, L.; Barrot, C.; Colin, S. Thermally driven pumps and diodes in multistage assemblies consisting of microchannels with converging, diverging and uniform rectangular cross sections. *Microfluid. Nanofluidics* **2020**, *24*, 1–17.
11. Gupta, N.K.; An, S.; Gianchandani, Y.B. A Si-micromachined 48-stage Knudsen pump for on-chip vacuum. *J. Micromech. Microeng.* **2012**, *22*, 105026. [CrossRef]
12. An, S.; Gupta, N.K.; Gianchandani, Y.B. A Si-Micromachined 162-Stage Two-Part A Si-Micromachined 162-Stage Two-Part Knudsen Pump for On-Chip Vacuum. *J. Microelectromech. Syst.* **2014**, *23*, 406–416. [CrossRef]
13. Byambadorj, T.; Cheng, Q.; Qin, Y.; Gianchandani, Y.B. A Monolithic Si-Micromachined 4-Stage Knudsen Pump for μGC Applications. *J. Micromech. Microeng.* **2021**, *31*, 034001. [CrossRef]
14. Healy, R.N.; Storvick, T.S. Rotational Collision Number and Eucken Factors from Thermal Transpiration Measurements. *J. Chem. Phys.* **1969**, *50*, 1419. [CrossRef]
15. Gupta, A.D.; Storvick, T.S. Analysis of the Heat Conductivity Data for Polar and Nonpolar Gases Using Thermal Transpiration Measurements. *J. Chem. Phys.* **1970**, *52*, 742. [CrossRef]
16. Jousten, K. (Ed.) *Handbook of Vacuum Technology*; WILEY-VCH Verlag GmBH & Co. KGaA: Weinheim, Germany, 2008.
17. Pavese, F.; Molinar, G.; Becient, M. *Modern Gas-Based Temperature and Pressure Measurements*, 2nd ed.; Springer: New York, NY, USA; Dordrecht, The Netherlands; Heidelberg, Germany; London, UK, 2013.
18. Hobson, J.P. Surface smoothness in thermal transpiration at very low pressures. *J. Vac. Sci. Technol.* **1969**, *6*, 257–259. [CrossRef]

19. Knudsen, M.; Partington, J. The Kinetic Theory of Gases. Some Modern Aspects. *J. Phys. Chem.* **1935**, *39*, 307. [CrossRef]
20. Weber, S.; Schimdt, G. *Experimentelle Untersuchungen über die thermomolekulare Druckdifferenz in der Nähe der Grenzbedingung* $p_1/p_2 = (T_1/T_2)^{1/2}$ *und Vergleichung der Theorie*; Kamerlingh Onnes Laboratory: Leiden, The Netherlands, 1936; p. 72.
21. Liang, S.C. Some Measurements of Thermal Transpiration. *J. Appl. Phys.* **1951**, *22*, 148. [CrossRef]
22. Liang, S.C. On the calculation of thermal transpiration. *J. Phys. Chem.* **1953**, *57*, 910–911. [CrossRef]
23. Los, J.M.; Fergusson, R.R. Measurements of thermomolecular pressure differences on argon and nitrogen. *Trans. Faraday Soc.* **1952**, *48*, 730–738. [CrossRef]
24. Takaishi, T.; Sensui, Y. Thermal transpiration effect of hydrogen, rare gases and methane. *Trans. Faraday Soc.* **1963**, *59*, 2503–2514. [CrossRef]
25. Annis, B.K. Thermal creep in gases. *J. Chem. Phys.* **1972**, *57*, 2898. [CrossRef]
26. Loyalka, S.K.; Cipolla, J.W., Jr. Thermal creep slip with arbitrary accommodation at the surface. *Phys. Fluids* **1971**, *14*, 1656–1661. [CrossRef]
27. Edmonds, T.; Hobson, J.P. A study of thermal transpiration using ultrahigh-vacuum techniques. *J. Vac. Sci. Technol.* **1965**, *2*, 182. [CrossRef]
28. Sharipov, F. Application of the Cercignani–Lampis scattering kernel to calculations of rarefied gas flows. III. Poiseuille flow and thermal creep through a long tube. *Eur. J. Mech. B/Fluids* **2003**, *22*, 145–154. [CrossRef]
29. Porodnov, B.T.; Kulev, A.N.; Tuchvetov, F.T. Thermal transpiration in a circular capillary with a small temperature difference. *J. Fluid Mech.* **1978**, *88*, 609–622. [CrossRef]
30. Sharipov, F.; Moldover, M.R. Energy accommodation coefficient extracted from acoustic resonator experiments. *J. Vac Sci. Technol. A* **2016**, *34*, 061604. [CrossRef] [PubMed]
31. Nguyen, N.N.; Graur, I.; Perrier, P.; Lorenzani, S. Variational derivation of thermal slip coefficients on the basis of the Boltzmann equation for hard-sphere molecules and Cercignani-Lampis boundary conditions: Comparison with experimental results. *Phys. Fluids* **2020**, *32*, 102011. [CrossRef]
32. Yamaguchi, H.; Perrier, P.; Ho, M.T.; Méolans, J.G.; Niimi, T.; Graur, I. Mass flow measurement of thermal creep flow from transitional to slip flow regime. *J. Fluid Mech.* **2016**, *795*, 690–707. [CrossRef]
33. Cercignani, C.; Lampis, M. Kinetic models for gas-surface interactions. *Transp. Theory Stat. Phys.* **1971**, *1*, 101–114. [CrossRef]
34. Cercignani, C. A variational principle for boundary value problems in kinetic theory. *J. Stat. Phys.* **1969**, *1*, 297–311. [CrossRef]
35. Cercignani, C.; Lampis, M.; Lorenzani, S. Plane Poiseuille-Couette problem in micro-electro-mechanical systems applications with gas-rarefaction effects. *Phys. Fluids* **2006**, *18*, 087102. [CrossRef]
36. Loyalka, S.K. Kinetic theory of thermal transpiration and mechanocaloric effect. I. *J. Chem. Phys.* **1971**, *55*, 4497–4503. [CrossRef]
37. Sharipov, F. Onsager-Casimir reciprocity relations for open gaseous systems at arbitrary rarefaction. I General theory for single gas. *Phys. A* **1994**, *203*, 437–456. [CrossRef]
38. Sharipov, F. Onsager-Casimir reciprocity relations for open gaseous systems at arbitrary rarefaction. II Application of the theory for single gas. *Phys. A* **1994**, *203*, 457–485. [CrossRef]
39. Cercignani, C.; Lampis, M.; Lorenzani, S. Variational approach to gas flows in microchannels. *Phys. Fluids* **2004**, *16*, 3426–3437. [CrossRef]
40. Cercignani, C.; Lorenzani, S. Variational derivation of second-order slip coefficients on the basis of the Boltzmann equation for hard-sphere molecules. *Phys. Fluids* **2010**, *22*, 062004. [CrossRef]
41. Lorenzani, S. High order slip according to the linearized Boltzmann equation with general boundary conditions. *Phylosophical Trans. R. Soc. A* **2011**, *369*, 2228–2236. [CrossRef] [PubMed]
42. Rojas Cardenas, M.; Graur, I.; Perrier, P.; Méolans, J.G. Thermal transpiration flow: A circular cross-section microtube submitted to a temperature gradient. *Phys. Fluids* **2011**, *23*, 031702. [CrossRef]
43. Rojas-Cardenas, M.; Graur, I.; Perrier, P.; Méolans, J.G. An experimental and numerical study of the final zero-flow thermal transpiration stage. *J Therm. Sci. Technol.* **2012**, *7*, 437–452. [CrossRef]
44. Rojas-Cardenas, M.; Graur, I.; Perrier, P.; Méolans, J.G. Time-dependent experimental analysis of a thermal transpiration rarefied gas flow. *Phys. Fluids* **2013**, *25*, 072001. [CrossRef]
45. Yamaguchi, H.; Rojas-Cardenas, M.; Perrier, P.; Graur, I.; Niimi, T. Thermal transpiration flow through a single rectangular channel. *J. Fluid Mech.* **2014**, *744*, 169–182. [CrossRef]
46. Méolans, J.G.; Nacer, M.H.; Rojas, M.; Perrier, P.; Graur, I. Effects of two transversal finite dimensions in long microchannel: Analytical approach in slip regime. *Phys. Fluids* **2012**, *24*, 112005. [CrossRef]
47. Graur, I.; Ho, M.T. Rarefied gas flow through a long rectangular channel of variable cross section. *Vacuum* **2014**, *101*, 328–332. [CrossRef]
48. Bird, G.A. *Molecular Gas Dynamics and the Direct Simulation of Gas Flows*; Oxford Science Publications; Oxford University Press Inc.: New York, NY, USA, 1994.
49. Ferziger, J.H.; Kaper, H.G. *Mathematical Theory of Transport Processes in Gases*; North-Holland Publishing Company: Amsterdam, The Netherlands, 1972.
50. Chapman, S.; Cowling, T.G. *The Mathematical Theory of Non-Uniform Gases*; University Press: Cambridge, UK, 1970.
51. Gross, E.P.; Ziering, S. Kinetic theory of linear shear flow. *Phys. Fluids* **1958**, *1*, 213–224. [CrossRef]

52. Gross, E.P.; Ziering, S. Heat flow between parallel plates. *Phys. Fluids* **1959**, *2*, 701–712. [CrossRef]
53. Wang Chang, C.; Uhlenbeck, G. *Transport Phenomena in Very Dilute Gases*; Technical Report CH-579, UMH-3-F; Engineering Research Institute, University of Michigan: Ann Arbor, MI, USA, 1949.